J. Fluid Mech. (2000), *vol.* 412, *pp.* 331–353. Printed in the United Kingdom

Vortex merging in quasi-geostrophic flows

By J. VON HARDENBERG[1], J. C. MCWILLIAMS[2], A. PROVENZALE[1], A. SHCHEPETKIN[2] AND J. B. WEISS[3]

[1]Istituto di Cosmogeofisica del CNR, corso Fiume 4, I-10133 Torino, Italy
[2]Institute of Geophysics and Planetary Physics, UCLA, Los Angeles, CA 90095-1567, USA
[3]PAOS, University of Colorado, Boulder, CO 80309, USA

(Received 26 April 1999 and in revised form 30 November 1999)

We study symmetric vortex merger in quasi-geostrophic flows using numerical simulations with high vertical resolution. We analyse the effect of varying the vertical aspect ratio of the vortices and compare with the barotropic case. During the merging of potential vorticity cores with small aspect ratio, we observe the birth of secondary instabilities on the filaments. This is a new phenomenon not seen in baroclinic simulations having low vertical resolution. Passive Lagrangian tracers are used to explore the transport of fluid parcels during vortex merger, to provide a detailed view of the flow evolution, and to determine the value of the critical merging distance for baroclinic vortices.

1. Introduction

Rotating turbulent flows are characterized by the presence of intense coherent vortices which contain a significant fraction of the energy and the enstrophy of the system and are nearly impermeable to inward and outward particle fluxes (see e.g. Bengtson & Lighthill 1982; McWilliams 1984, 1989, 1990; Flierl 1987; McIntyre 1989; Ingersoll 1990; Elhmaidi, Provenzale & Babiano 1993; Hopfinger & van Heijst 1993; Babiano *et al.* 1994; McWilliams, Weiss & Yavneh 1994, 1999; Provenzale 1999). These vortices live much longer than a typical eddy turnover time and intermittently undergo strongly dissipative, non-reversible (inelastic) interactions with each other, see e.g. Dritschel (1995) for the case of barotropic turbulence. The mechanisms of inelastic interaction have been shown to be of central importance for the evolution of the statistical characteristics of the flow, see e.g. Carnevale *et al.* (1991) and Weiss & McWilliams (1993) for two-dimensional turbulence and McWilliams *et al.* (1999) for baroclinic quasi-geostrophic (three-dimensional) turbulence.

In two-dimensional turbulence, like-sign vortex merger is the primary interaction responsible for the evolution of the vortex population, and it is associated with the inverse energy cascade from small to large scales (e.g. Kraichnan & Montgomery 1980). Conversely, the direct cascade of enstrophy from large to small scales takes place mainly through strong filamentation events, which ultimately lead to enstrophy dissipation.

In quasi-geostrophic three-dimensional turbulence, similar cascades take place. Here as well, the properties of same-sign vortex merging determine the flow evolution, together with the new possibilities of merging of vortices on slightly different vertical

levels and of vortex alignment, during which vortices on different levels settle on a common vertical line (McWilliams 1989; McWilliams & Weiss 1994; McWilliams *et al.* 1994, 1999; Sutyrin, McWilliams & Saravanan 1998).

Owing to its importance in controlling the evolution of rotating flows, the problem of a proper understanding of vortex merging has stimulated widespread interest. Vortex merging has been studied in depth in the two-dimensional case (see e.g. Zabusky, Hughes & Roberts 1979; Melander, Zabusky & McWilliams 1987, 1988; Waugh 1992; Dritschel 1995; Nielsen *et al.* 1996; Kevlahan & Farge 1997), where the problem of the symmetric merger of equal patches of relative vorticity has received particular attention. One of the main results of these studies is the identification of a 'critical merging distance', d_c, below which two equal-vorticity patches merge to form a single, nearly axisymmetric, final vortex. For two identical patches of constant relative vorticity on an infinite plane one finds $d_c \approx 3.3R$ where R is the initial radius of the patches.

The merging of quasi-geostrophic baroclinic vortices has been explored less thoroughly, mainly focusing on the simplified case of two-layer systems (Griffiths & Hopfinger 1987; Polvani, Zabusky & Flierl 1989; Verron, Hopfinger & McWilliams 1990; Verron & Hopfinger 1991; Verron & Valcke 1994; Valcke & Verron 1997). An interesting problem here concerns the role of stratification. The laboratory experiments of Griffiths & Hopfinger (1987) on stably-stratified two-layer rotating fluid have indicated that the conditions for merging strongly depend on the type of stratification. Later on, however, numerical simulations by Polvani *et al.* (1989) indicated that stratification does not significantly affect the properties of vortex merging in two-layer quasi-geostrophic flows, thus opening an intriguing discrepancy with the experimental results. These results were reconsidered by Verron *et al.* (1990), who solved the discrepancy by showing the importance of the type of initial conditions. In fact, the results of Polvani *et al.* (1989) were obtained by starting with two equal patches of potential vorticity in one layer, keeping a constant reservoir of potential vorticity in the other layer (what is called a PVI initialization). In this case, the strength of stratification does not significantly affect vortex merging. However, stratification does play an important role if one starts with two anomalies of relative vorticity in one layer, and zero vorticity in the other (what is called RVI initialization, and the one that was used in the laboratory experiments). The implications of these results and an intermediate form of initialization are discussed further by Verron & Hopfinger (1991).

From the above discussion, it is clear that the vertical structure of the initial conditions plays an important role in the merging process. In the case of low vertical resolution (two layers), it is hard to properly resolve the vertical structure of the vortices, and the extreme conditions of RVI and PVI initializations are encountered when trying to define baroclinic initial conditions in such a minimal system. An alternative and physically more interesting possibility is to raise the vertical resolution, obtaining a better definition of the detailed structure of the flow. In the present work, we adopt this approach and focus on the study, using high vertical resolution, of the merging of identical, ellipsoidal, cosine-shaped PV distributions centred on the same vertical level (symmetric merger).

The rest of this paper is organized as follows. In § 2 we give a short introduction to the quasi-geostrophic approximation and we describe our approach to the study of vortex merging. Sections 3 and 4 contain the discussion of the Eulerian and Lagrangian aspects of the merging process. Finally, § 5 gives conclusions and perspectives.

2. Physical and numerical background

2.1. *The quasi-geostrophic approximation*

The quasi-geostrophic (QG) equations represent an approximation to the primitive equations in the case of rapidly rotating and stably stratified fluid (e.g. Pedlosky 1987). As such, they are relevant to large-scale planetary geophysical flows in the atmosphere and the oceans when relative vorticity is much smaller than planetary vorticity.

Important non-dimensional parameters of the problem are the Rossby number

$$\mathscr{R}o = \frac{U}{fL}, \tag{1}$$

where L and U are characteristic length and velocity scales of the fluid motion; f is the Coriolis parameter defined as $f = 2\Omega \cdot \boldsymbol{n}$, where Ω is the rotation rate of the Earth and $\boldsymbol{n}$ is the unit vector in the local vertical direction; and the Burger number,

$$\mathscr{B}u = \left(\frac{NH}{fL}\right)^2, \tag{2}$$

where

$$N^2(z) = -\frac{g}{\rho}\frac{\partial \rho}{\partial z} \tag{3}$$

is the Brunt–Väisälä (buoyancy) frequency, g is the acceleration due to gravity, ρ is the fluid density and H is a typical vertical scale of motion.

In the quasi-geostrophic approximation, the Rossby number is assumed to be small, $\mathscr{R}o \ll 1$, while the Burger number, although typically less than one for atmospheric and oceanic vortices, is not necessarily assumed to be small.

In this approximation, and assuming no external forcing, the equation of fluid motion becomes

$$\frac{\mathrm{D}q}{\mathrm{D}t} \equiv \frac{\partial q}{\partial t} + J(\psi, q) = \mathscr{D}, \tag{4}$$

where

$$J(\psi, q) = \frac{\partial \psi}{\partial x}\frac{\partial q}{\partial y} - \frac{\partial \psi}{\partial y}\frac{\partial q}{\partial x}$$

is the Jacobian operator, ψ is the stream function and the potential vorticity q is defined as

$$q = \frac{\partial^2 \psi}{\partial x^2} + \frac{\partial^2 \psi}{\partial y^2} + \frac{\partial}{\partial z}\frac{1}{S(z)}\frac{\partial \psi}{\partial z}, \tag{5}$$

where $S(z) = N^2(z)/f^2$ represents the strength of the stratification. The term $\mathscr{D}$ on the right-hand side of (4) represents dissipative processes, which are assumed to be small compared with the other terms. Explicit forms of the dissipation are discussed in the next subsection. In the absence of dissipation, (4) states the conservation of potential vorticity q for each fluid particle.

At the order of the QG approximation, vertical velocities vanish and the horizontal velocity $\boldsymbol{u} = (u, v)$ is non-divergent. This is defined by

$$u = -\frac{\partial \psi}{\partial y}, \qquad v = \frac{\partial \psi}{\partial x}. \tag{6}$$

Numerical simulations of vortex dynamics in quasi-geostrophic turbulence have been discussed by Hua & Haidvogel (1986), McWilliams (1989), Meacham (1993),

McWilliams & Weiss (1994), McWilliams *et al.* (1994), Dritschel & Saravanan (1994), Meacham *et al.* (1994), Sutyrin *et al.* (1998), McWilliams *et al.* (1999).

In the case of uniform stratification, $S = \text{const.}$, it is possible to introduce a stretched coordinate system where the vertical coordinate is rescaled as $z \to z' = (N/f)z$. In the new variables, the right-hand side of (5) becomes the isotropic three-dimensional Laplacian operator,

$$q = \nabla^2\psi, \quad \text{where} \quad \nabla^2 = \frac{\partial^2}{\partial x^2} + \frac{\partial^2}{\partial y^2} + \frac{\partial^2}{\partial z'^2}. \tag{7}$$

A well-known prediction by Charney (1971) claims that the solutions in the stretched coordinate frame should be statistically isotropic in the inertial range. Numerical simulations by McWilliams *et al.* (1994) have shown that this prediction is only approximately verified in that an initially random isotropic spectrum evolves into an anisotropic spectrum, and that the self-organization of vortices and subsequent merging and alignment processes result in slighly flattened ellipsoidal vortices rather than spherical ones (in rescaled coordinates).

2.2. *The numerical model*

The numerical code used to integrate the Eulerian equation of motion, (4), is based on the finite difference method discussed by Shchepetkin & McWilliams (1998). In this approach, an F-cycle correction scheme, multigrid elliptic solver is used to invert the discrete analogue of (5), see e.g. Yavneh & McWilliams (1995). A third-order-accurate predictor-corrector (Leap-Frog–Adams-Moulton III) scheme is used for time stepping, while both spatial derivatives and spatial interpolations in the advection operator are kept accurate at sixth order. The discretization scheme for the Jacobian operator in (4) is cast into flux-divergent form and it keeps a high degree of spatial isotropy by retaining fluxes along the grid as well as diagonal fluxes, similarly to the classical Arakawa Jacobian.

In any numerical integration of turbulent flow, a basic problem is to achieve a Reynolds number that is as large as possible, while keeping the solution relatively smooth on the grid scale. To deal with this issue, in most previous studies a *hyper*viscosity operator has been used to parametrize subgrid dissipative processes, $\mathscr{D} = (-1)^{p+1}\nu_p\nabla^{2p+2}\psi$ where $p = 1, 2\ldots$. The values of the coefficient ν_p and of the power p are dictated by the compromise between the desire to have minimal dissipation and the necessity of keeping the solution smooth on the grid scale. For $p \geqslant 2$ this is often referred to as scale-selective dissipation.

For a given grid resolution, it is possible to reach even smaller overall dissipation by resorting to an explicit locally adaptive dissipation (ELAD) technique, see Shchepetkin & McWilliams (1998). This approach is based on the 'principle of monotonicity' for the advection equation, which postulates that an advected quantity (such as potential vorticity in (4)) may only be: (i) conserved along the trajectory of each fluid particle, and (ii) diffused, satisfying the local maximum principle for the diffusion equation. For the discretized version of equation (4), this procedure first performs an inviscid time step, then it checks (at every grid point) whether the value of the newly computed PV field lies within pre-selected permissible bounds based on the minimum and maximum values of the field at the previous time step and at neighbouring points in the upstream direction. If the limits are exceeded (either above or below), the excess PV values (overshoots) are diffused in a conservative manner by distributing them among neighbouring points. In principle, this requires several iterations, as the entire procedure should be repeated until all the newly computed potential vorticity values

lie within the permissible bounds. In practice, in most cases only a few iterations are sufficient. In the present study we use eight diffusive iterations at each time step.

In addition to ELAD, we also employ an 'extrema discriminating' algorithm. It is well-known (e.g. Leonard 1979), that any total variation diminishing (TVD) algorithm, while preserving monotonicity in the profiles of advected quantities, causes artificial truncation of narrow extrema. The goal of an extrema discriminating algorithm is to distinguish between narrow physical extrema and spurious extrema generated by dispersive overshoot in the advection scheme. To this end, here we use a criterion discussed by Shchepetkin & McWilliams (1998), based on checking the convexity of the profile of the advected quantity (here, PV) along a line of six grid points centred on the extremum. If the finite-difference, discrete analogue of the second derivative keeps the same sign along four consecutive grid points, then the tested extremum is accepted as physical. In this case, the permissible bounds around this point are relaxed, and the amount of dissipation is locally reduced. By contrast, if the second derivative changes sign, the permissible bounds are kept as defined by the standard ELAD algorithm, and the extremum will be reduced or suppressed in the following iteration. The mathematical background of this approach is the fact that dispersive errors generated by high-order-accurate advection schemes have oscillatory patterns with wavelength close to or slightly larger than twice the grid spacing, and will thus be classified as spurious extrema, while the physical extrema (which must be properly propagated by the advection scheme) occur on scales larger than a few grid points.

We believe that whereas the general characteristics of the merging process should not be affected by the specific choice of the dissipation scheme, a locally adaptive scheme deals better with the small-scale structures which form during merging. In order to reach high resolution, the numerical code has been parallelized to run on shared-memory parallel machines. Simulations with a moderate vertical resolution (up to 64 levels) easily run on single-processor work stations.

2.3. *Setup of the numerical experiments*

In the following, we consider a domain with horizontal size 2π and rescaled vertical size D. Thus, $0 \leqslant (x, y) < 2\pi$ and $0 \leqslant z' = Nz/f < D$. In all the cases considered, we use a constant Brunt–Väisälä frequency $N(z) = N_0$. We use periodic boundary conditions in both horizontal and vertical directions, and the vertical extent D of the domain is chosen to ensure that the merging vortices are sufficiently far away from the boundaries. Note that, since we consider PV fields that are symmetric with respect to the mid-plane $z'_c = D/2$, no-stress and periodic vertical boundary conditions provide the same results.

The horizontal resolution is set to $N_h = 256$ grid points for the general runs and to $N_h = 128$ for the exploration of the critical merging distance (see § 4.4); the vertical resolution N_z is varied between 16 and 256 levels. The time step is chosen such that the CFL number never exceeds $\frac{1}{4}$ during the whole evolution. In order to compare cases with different vertical aspect ratio, and to have approximately the same time scales for horizontal motions of advected tracers, we have normalized the maximum PV in each simulation such that the initial kinetic energy on the central horizontal plane $z'_c = D/2$ assumes a fixed value:

$$\langle E \rangle_{z'_c} = \frac{1}{2(2\pi)^2} \iint \left[\left(\frac{\partial \psi}{\partial x} \right)^2 + \left(\frac{\partial \psi}{\partial y} \right)^2 \right] \mathrm{d}x \, \mathrm{d}y = 0.5. \tag{8}$$

The initial conditions for the merging process are provided by two ellipsoidal PV

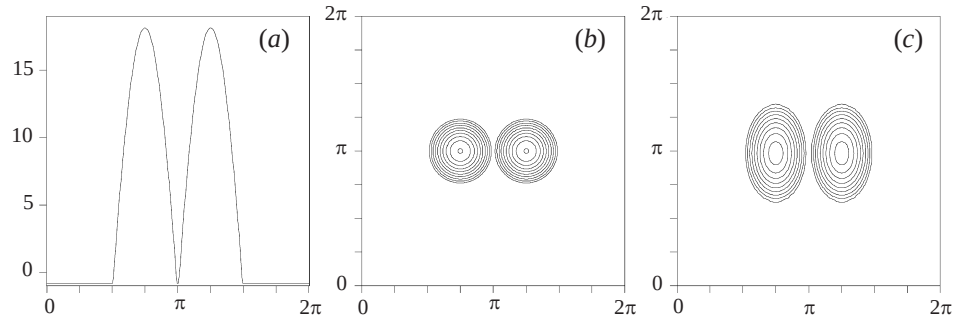

FIGURE 1. Initial PV distribution: (*a*) the cosine profile of the vortices, (*b*) horizontal PV section on the mid-plane $z'_c = D/2$, (*c*) vertical PV section on the plane (x, z).

N_z	H/R	D	T_{max}
1	∞	(barotropic)	24
256	1.50	2π	20
256	0.66	2π	20
256	0.585	2π	50
64	2.50	2π	20
64	0.66	2π	20
64	0.16	$\pi/2$	20

TABLE 1. Values of the vertical resolution N_z, vertical aspect ratio H/R, vertical physical domain size D and maximum time T_{max} for the simulations with horizontal resolution $N_h = 256$ discussed in the text.

distributions, having circular horizontal cross-sections with radius $R = \pi/4$ at the mid-plane and half-height H, defining the initial vertical aspect ratio H/R. The PV profile has a cosine shape, and the centres of the two PV distributions are located on the central plane $z'_c = D/2$ at distance d from each other. In most experiments, in order to have rapid merging, we fix d well below the critical merging distance. For $d = 2R$, a value we often use, the two initial vortices touch each other at the centre of the domain. Figure 1 shows the initial PV profile, and the initial horizontal and vertical cross-sections through the centre of the domain.

After generating the initial PV distribution, the mean PV value must be subtracted from the original field, as needed to solve the Poisson equation (5) with periodic boundary conditions. Indeed, since the quasi-geostrophic equations are invariant under addition of a function of the vertical coordinate, we redefine PV on each vertical level as (Yavneh & McWilliams 1995)

$$q' = q - \langle q \rangle_h(z) \quad \text{where} \quad \langle q \rangle_h(z) = \frac{1}{(2\pi)^2} \iint q \, \mathrm{d}x \, \mathrm{d}y, \tag{9}$$

and similarly for the stream function.

The various cases described below correspond to different choices of the vertical aspect ratio H/R, vertical domain size D and vertical resolution N_z, as summarized in table 1. Note that changing the vertical aspect ratio of the initial vortices is equivalent to changing the strength of the stratification. Recalling that the vertical coordinate is $z' = Nz/f$, it is clear that a change in H (with $L = 2\pi$ and R constant) can be due to either a change in the vertical size of the vortex or a change in N/f.

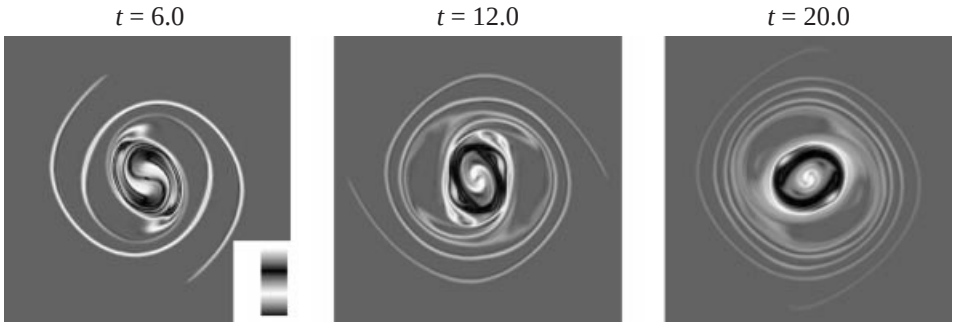

FIGURE 2. Relative vorticity at times $t = 6, 12, 20$ for the barotropic case.

3. Vortex merging: Eulerian analysis

3.1. *Role of the vertical stratification*

One of the main goals of this work is to study how the strength of the vertical stratification affects the merging process. To this end, we consider simulations with different values of the initial vertical aspect ratio, H/R, while keeping a fixed stratification, $N/f = 1$.

We start our analysis by first considering, as reference, barotropic vortex merging. Thus, we generate two initially circular distributions of relative vorticity and integrate (4) with one vertical layer and periodic boundary conditions. The two vortices have initial radius R and their centres are at a distance $d = 2R$. Thus, the vortices initially touch each other. For consistency, these two-dimensional vortices have the same kinetic energy as the three-dimensional vortices in the central horizontal plane.

Figure 2 shows the vorticity field for the barotropic case at different instants of time. Starting from an initial distance which is well below the 'merging threshold' (Polvani *et al.* 1989), the two vortices merge rapidly to form a single final core surrounded by thin vorticity filaments. As discussed by Melander *et al.* (1987), the merging can be described as an axisymmetrization process where the merging vortices, owing to the inviscid conservation of circulation, expel excess angular momentum through filamentation. The filaments do not undergo any further instability and they are slowly destroyed by dissipation.

We now consider the merging process for three-dimensional vortices with vertical aspect ratio $H/R = 1.5$ in a domain with vertical size $D = 2\pi$. Figure 3(a) shows horizontal sections of potential vorticity on the mid-plane $z'_c = D/2$, where the vortices reach their maximum horizontal extent. Figure 3(b) shows horizontal sections of the PV distribution at a height of $z'_1 = z'_c + 3H/4$, and 3(c) shows vertical sections of the PV field, on the plane $y = \pi$. These latter images show that what appeared as filaments in a horizontal section is actually an ensemble of 'PV sheets' shed off by the merging cores, which curve to engulf the merging vortices.

Any similarity with the barotropic case breaks down when we look at what happens above or below the central horizontal plane. At the height z'_1, the two initial PV distributions form two circles of PV which are at a distance of about 3 radii from each other (not shown). In a barotropic flow, this would be about the critical distance for merger. Above this value, we would expect two barotropic vortices to simply orbit around each other. In the present case, however, the baroclinic coupling with the lower levels induces the two cores to elongate into a spiral-like shape, neither merging in a central vortex nor remaining unperturbed. At heights corresponding

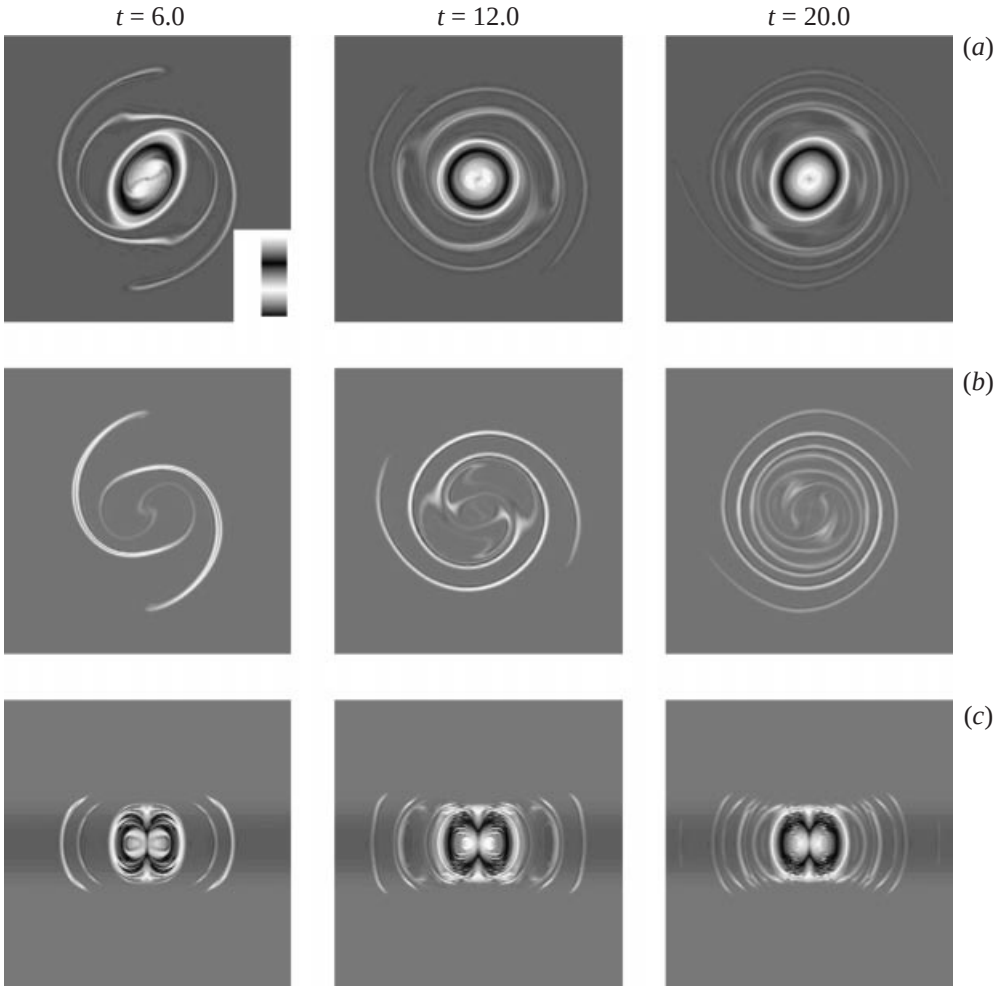

FIGURE 3. Potential vorticity distribution for baroclinic merging with vertical aspect ratio $H/R = 1.5$ at times $t = 6, 12, 20$. (*a*) Horizontal sections of potential vorticity on the mid-plane $z_c' = D/2$; (*b*) horizontal sections of potential vorticity on the plane $z_1' = \frac{1}{2}D + \frac{3}{4}H$; (*c*) vertical sections of potential vorticity on the plane (x, z).

to the top of the vortices, PV is shaped into a spiral and nothing is left to form a final core. As evident from figure 3, together with the necessary increase of the final vortex radius due to conservation of circulation, this leads to an effective decrease of the final vortex height with respect to its initial value, and thus to a decrease of the vertical aspect ratio. We return to this point in § 3.2.

As suggested by figure 3, the PV sheets form a spiralling envelope around the merged vortices, showing an unexpected amount of structure. However, the vertical curvature of the filaments (as seen in figure 3*c*) is not an intrinsically baroclinic effect. To verify this, we have studied the evolution of an ensemble of superposed two-dimensional layers, independent of each other, each having as initial condition the PV distribution appropriate for that level. That is, we have artificially cut the vertical coupling in (4), by dropping the vertical derivative in the definition of the potential vorticity (5). In the resulting PV field, the filaments display a 'vertical' curvature which

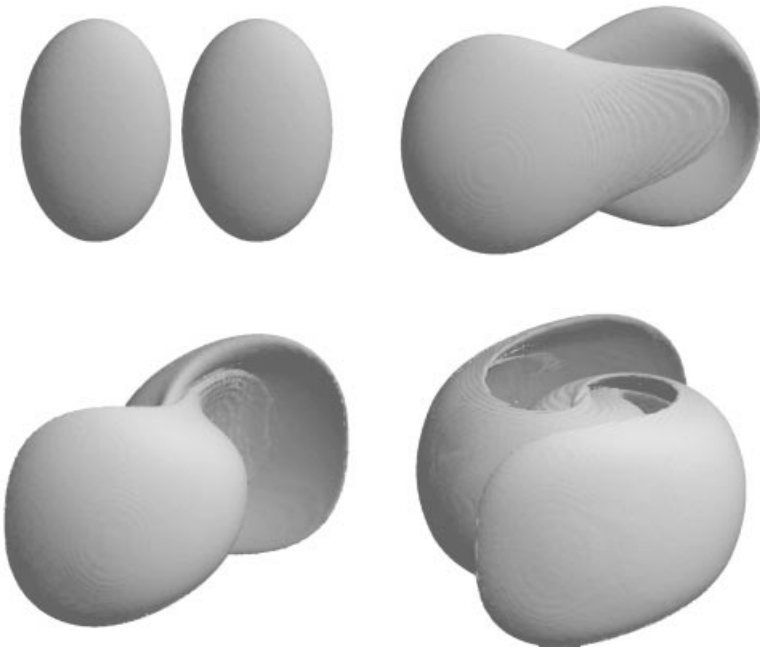

FIGURE 4. Volume rendering of potential vorticity at times $t = 0, 1, 2, 4$ for baroclinic merging with $H/R = 1.5$.

is similar to that observed in the three-dimensional case. The vertical curvature of the filaments is generated only by the fact that the PV distribution is different at different levels, thus inducing a different dynamic time scale in each layer. Indeed, the result that small scales are not strongly coupled in the vertical makes sense from the nature of the inversion operator.

Another interesting aspect concerns the dynamics of the central vortex cores, which evolve into an elongated shape, with a faster and thinner handle preceding a curved and flattened core (a sort of spoon-like shape). The core then thins out and evolves to form the filaments which are shed off. This behaviour is different from what happens in the barotropic case, where there is no fast-moving handle preceding the core. A three-dimensional rendering of the PV field, shown in the four panels of figure 4, illustrates the structure of the merging vortex cores.

At a larger vertical aspect ratio, $H/R = 2.5$, the picture is substantially unaltered. At lower aspect ratios, however, novel features appear. For initially flatter vortices, with $H/R = 0.66$, the vorticity filaments shed during the merging process develop secondary instabilities and small second-generation vortices appear along the filaments. Figure 5 shows three horizontal (*a*) and vertical (*b*) sections of the PV field at different instants of time. The filaments still have a vertical curvature as for larger aspect ratios, but in addition the newly formed vortices are visible along the filaments.

This phenomenon is even stronger for flatter vortices, as demonstrated in figure 6 for aspect ratio $H/R = 0.16$. In this case, the filaments are almost completely destroyed by the instability and the second-generation vortices dominate the PV distribution far from the central core.

To better understand the nature of this instability we have analysed in detail the process leading to the formation of a secondary vortex. We defined a small region around the location where the vortex forms and calculated the barotropic energy

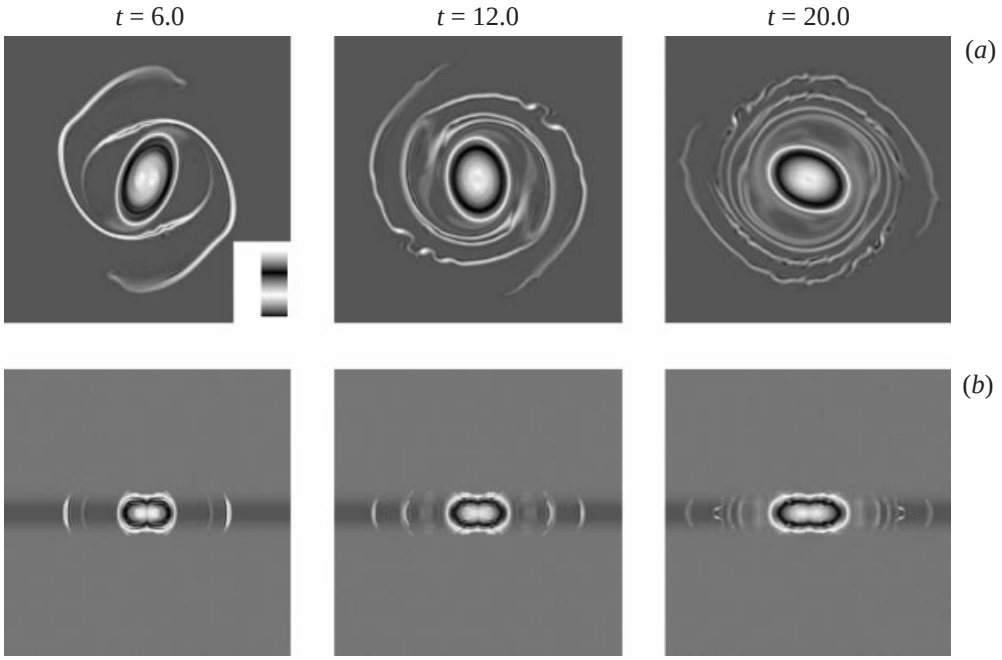

FIGURE 5. Potential vorticity distribution for baroclinic merging with vertical aspect ratio $H/R = 0.66$ at times $t = 6, 12, 20$. (*a*) Horizontal sections of potential vorticity on the mid-plane $z_c' = D/2$; (*b*) vertical sections of potential vorticity on the plane (x, z).

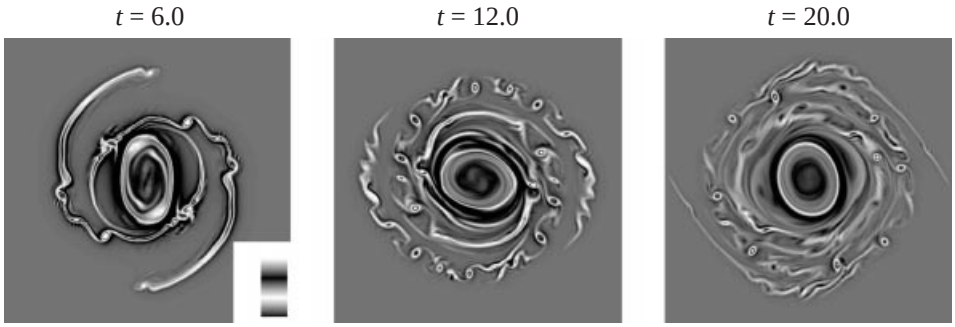

FIGURE 6. Potential vorticity distribution for baroclinic merging with vertical aspect ratio $H/R = 0.16$. The panels show horizontal sections of potential vorticity at times $t = 6, 12, 20$ on the mid-plane $z_c' = D/2$.

conversion term $\overline{u'v'}\partial_y u_0$ and the baroclinic energy conversion term $S(z)^{-1}\overline{v'\partial_z \psi'}$. Here u' and v' are respectively the tangential and radial velocity anomalies, $u_0 = \overline{u}$, and an overbar denotes local averaging in the tangential direction (e.g. Pierrehumbert & Swanson 1995). Figure 7(*b*) shows the amplitude of the barotropic and baroclinic energy conversion terms along the portion of the filament indicated by the box in figure 7(*a*). The energy conversion terms are herein obtained as integrals along the direction perpendicular to the filament (approximated by x) and plotted as a function of y. The different magnitude of the two energy conversion terms suggests that the instability is mainly due to barotropic shear instability, without a significant baroclinic effect.

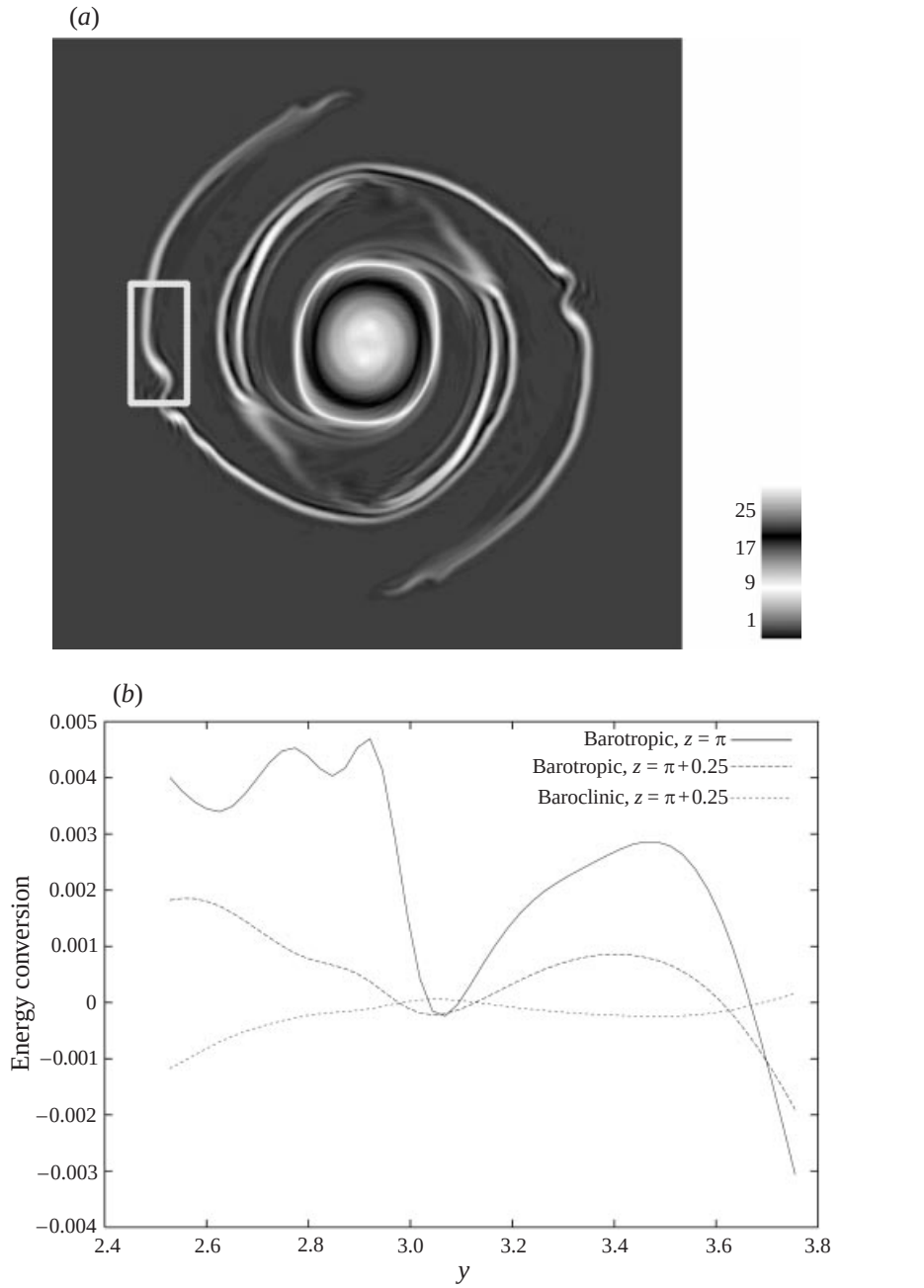

FIGURE 7. Barotropic and baroclinic energy conversion terms in filament instability for $H/R = 0.66$ at time $t = 10$. (*a*) Horizontal PV section on the central plane z'_c. The small box indicates the area of study. (*b*) Barotropic energy conversion at $z'_c = D/2$, barotropic energy conversion at $z'_1 = D/2 + 3H/4$, and baroclinic energy conversion at z'_1, integrated along x and plotted as a function of y.

Given that the instability of the filaments is a barotropic process, one may wonder why the same instability is absent in purely barotropic flows. For two-dimensional turbulence, adverse shear (Dritschel 1989) and strain (Dritschel *et al.* 1991) generated by a central vortex have been suggested to stabilize vorticity filaments. Along these

lines, Kevlahan & Farge (1997) have numerically shown that merging barotropic vortices do indeed stabilize vorticity filaments emitted during merger. Clearly, this mechanism is not at work for flat baroclinic vortices. One possible explanation relies upon the fact that the interactions are much more local in baroclinic flows, as may be seen from the different form of the Green's function, $G_{3D}(r) \propto 1/r$ at small r, compared to the barotropic form $G_{2D}(r) \propto \log r$. In quasi-geostrophic turbulence, the stream-function field generated by an isolated, three-dimensional point vortex centred on $r = (x^2+y^2+z'^2)^{1/2} = 0$ in a stratified fluid with constant N/f is $G_{3D}(r) \propto 1/r$. This corresponds to an induced velocity field with strength proportional to $1/r^2$. From this expression, one can recover the barotropic case by considering a line vortex aligned with the vertical axis, z', and integrate the baroclinic Green's function along z'. One then obtains the barotropic Green's function $G_{2D} \propto \log r$, which gives a velocity field with strength proportional to $1/r$. As a consequence, whereas in the barotropic case the adverse shear and strain fields induced by the central vorticity core are able to stabilize the filaments, in the three-dimensional case the more local interactions prevent this possibility and the filaments become shear unstable. This interpretation agrees with the results of Waugh & Dritschel (1991), who studied filament dynamics around merging vortices for a variety of Green's functions, including one approximating the $1/r$ behaviour of the three-dimensional Green's function at large r. The present results confirm that it is indeed the shorter range of the interaction that leads to filament instability.

The behaviour of flat QG vortices has interesting similarities with the evolution of vorticity filaments in surface quasigeostrophic dynamics (SQG), see e.g. Held *et al.* (1995), which describes the advection of a scalar field (e.g. temperature) by an infinite reservoir of uniform PV. The Green's function for SQG dynamics has the same form as that for a point vortex element in three-dimensional quasi-geostrophic flows. The simulations of Held *et al.* (1995) indicated that the free evolution of random initial conditions in the SQG approximation leads to the formation of coherent vortices that interact with each other, undergoing filamentation processes that are not too dissimilar from what is observed in barotropic turbulence. In SQG, however, the filaments become shear unstable, and roll up into vortices which then generate other unstable filaments at smaller scales. This process leads to a cascade of instabilities associated with the presence of several generations of vortices.

The SQG dynamics represents a good approximation to the three-dimensional dynamics studied here in the limit $H/R \to 0$, i.e. for flat vortices. For vortices with finite vertical extent, the Green's function at a given horizontal position is obtained by integrating over the vertical extent of the vortex. For vortices with small vertical aspect ratio, such as those depicted in figures 4 and 5, at large distances from the core the vertical extent of the vortex is unimportant, and the Green's function resembles that of SQG dynamics, $G_{3D} \propto 1/r$. Thus, one observes filament instabilities and generation of smaller vortices. At small distance from the vortices, however, the vertical extent of the vortices cannot be overlooked, and the appropriate stream-function field has to be obtained by integrating over the vortex height. This leads to a slower decay of the velocity field close to the vortex, and to a strain field that is strong enough to prevent the instability. Thus, one obtains a natural regularization of the potential ultraviolet catastrophe of SQG and observes only a finite number of generations of secondary vortices.

As a final comment we note that simulations with lower vertical resolution (64 layers) have provided analogous results, indicating that we have satisfactorily resolved the vertical structure of the merging vortices.

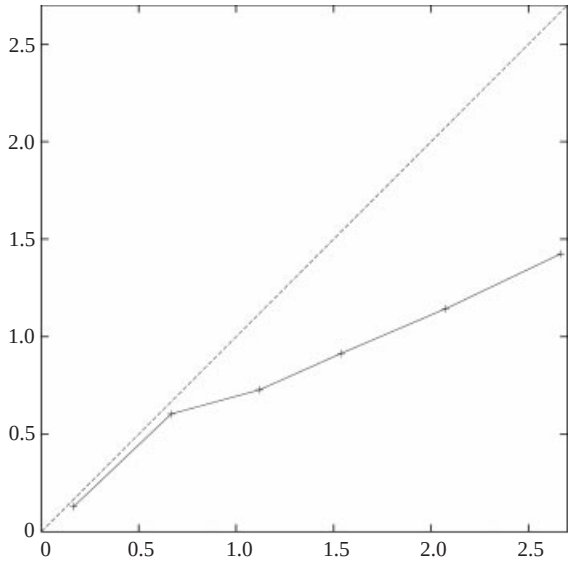

FIGURE 8. Final vertical aspect ratio H/R of a merged vortex versus its value for the two initial vortices.

3.2. *Evolution of the vertical aspect ratio*

The study of freely-decaying three-dimensional quasi-geostrophic turbulence evolving from random initial conditions has indicated, at intermediate times, the appearance of a vortex population characterized by approximate horizontal axisymmetry, ellipsoidal shape and preferred vertical aspect ratio $H/R \approx 0.8$ (McWilliams & Weiss 1994; McWilliams *et al.* 1994, 1999).

In this type of three-dimensional turbulence both vortex merging and vortex alignment play a role in the evolution of vortex statistics. Vortex alignment and merging of vortices on different vertical levels tend to increase the average vertical aspect ratio of the population (McWilliams *et al.* 1994; Sutyrin *et al.* 1998). On the other hand, the merging of vortices on the same level seems to provide a competitive, efficient mechanism for limiting the vertical size of the evolving vortices. Here we find that the merging of tall ($H/R = 1.5, 2.5$) vortices leads to a final core with smaller vertical aspect ratio, due to the filamentation of the PV distribution at the levels far away from the central plane. Nothing like this is observed when the vortices are flatter ($H/R = 0.66, 0.16$). In this case, even though we could *a priori* expect an increase of the vortex radius after merging and no increase in vortex height (thus, a decrease of H/R), the vertical aspect ratio does not grow during the merging, indicating that a significant fraction of the merged vortex has been first filamented and then dissipated. In figure 8 we show the value of the vertical aspect ratio H/R after merging versus its initial value, for a number of cases. The values of H and R used to define the aspect ratios reported in figure 8 are obtained by determining, for each initial and final (merged) vortex, the surface inside which potential vorticity, averaged inside the vortex, becomes 5% of its maximum value at the centre of the vortex. The value of H is one-half of the largest vertical extent of this surface, while the value of R is one-half of the largest horizontal extent of the surface.

Whenever $H/R \geqslant 1$ initially, we observe a tendency toward a smaller value at the end of the merging process, while H/R is approximately constant when it is initially

less than one. Note, in particular, that initially spherical vortices ($H/R = 1$) evolve into a final vortex which is a flattened ellipsoid, indicating that isotropy (in rescaled coordinates) is not preserved in vortex merging, in agreement with the obervations of McWilliams *et al.* (1999).

We suggest that this mechanism, which effectively accelerates the decrease of the vertical aspect ratio during the merging of tall vortices, could significantly limit the vertical size of the vortices during the evolution of freely-decaying three-dimensional quasi-geostrophic turbulence, leading, together with vortex alignment, to a vortex population with slightly flattened shape in rescaled coordinates $(x, y, Nz/f)$. This population of vortices is presumably typical of the period during which self-similar decay is present (McWilliams *et al.* 1999).

4. Vortex merging: Lagrangian analysis

4.1. *Motivation and setup*

In the previous section, we have provided a characterization of merging in a standard Eulerian framework. The dynamics of fluid particles during the merging event provides a complementary Lagrangian picture of the merging process.

To obtain a Lagrangian picture of vortex merging, we randomly distribute 32 768 passive particles in two circles with radius R, corresponding to the two initial PV cores, on the central horizontal plane $z_c' = D/2$. In the quasi-geostrophic approximation, the flow is in hydrostatic equilibrium and the vertical velocity vanishes, $w = 0$. This implies that the particle motion is purely horizontal, and it is described by the equations

$$\frac{\mathrm{d}x}{\mathrm{d}t} = -\frac{\partial \psi}{\partial y}, \qquad \frac{\mathrm{d}y}{\mathrm{d}t} = \frac{\partial \psi}{\partial x}, \tag{1}$$

where $(x(t), y(t))$ is the particle position at time t and $(-\partial\psi/\partial y, \partial\psi/\partial x)$ is the horizontal velocity. We numerically integrate the tracer dynamics by employing a leap-frog scheme with a periodic correction phase to damp the computational mode and a fourth-order local interpolator to obtain the velocity at the tracer position. As shown by Zouari & Babiano (1990), local bilinear interpolation is insufficient to provide reliable individual particle trajectories.

4.2. *Core structure*

Lagrangian tracers provide a detailed picture of the evolution of the vortex cores during merging. Figure 9(*a–d*) shows the distribution of passive particles at successive evolutive times, for (*a*) the barotropic case, and for baroclinic situations with aspect ratio (*b*) $H/R = 1.5$, (*c*) $H/R = 0.66$, and (*d*) $H/R = 0.16$. For both two-dimensional and three-dimensional flows, the particle populations initially placed in the merging vortices wrap around each other, keeping their identities for long times. Mixing of particle populations takes place only on diffusive time scales.

The interface between the two merging cores, however, evolves differently under barotropic and baroclinic conditions. In the two-dimensional case, this interface is S-shaped and winds up at later times to form a simple spiral with a leading bulky core. For three-dimensional merging, the interface has a more complicated shape. In this case, the 'tongue' that preceeds the vortex core is clearly visible, and a double spiral structure is created inside the final core. Due to the more convoluted interface between the two particle populations, diffusive effects can act more rapidly to homogenize the final particle distribution in baroclinic merging.

In the case with unstable vorticity filaments ($H/R = 0.66$), the tracers clearly mark the secondary vortices which form on the filaments. Some of these second generation vortices trap tracers for long times, analogously to what happens for barotropic vortices.

4.3. *Core entrainment*

In the process of vortex merging, it is interesting to identify the source region for the fluid that ends up in the final core. To address this point we have uniformly seeded 256^2 tracer particles, on both the central level of the domain, $z_c' = D/2$, and at $z_1' = z_c' + \frac{3}{4}H$, and we have followed their evolution up to the time $T_{max} = 20$ (our 'final' state).

For simplicity, we discuss only the case $H/R = 1.5$, as the cases for smaller vertical aspect ratio do not introduce new effects for this specific issue. Figure 10(*a*) shows the initial distribution of particles, where each tracer has been assigned a grey-scale coding that represents its final distance from the centre of the final (merged) vortex. The grey scale has been defined to clearly distinguish tracers which ended up inside the final vortex from those which remained outside.

On the mid-plane $z_c' = D/2$, the particles ending in the final vortex originate mainly from the cores of the merging vortices, plus a small contribution from two highly-structured external lobes. Analogously, almost all the particles which were initially in the cores of the merging vortices end up in the core of the final vortex. The hyperbolic point between the two initial cores may be clearly seen at the centre of the figure, as it is identified by diverging and converging streaks of tracers, crossing each other at the centre of the domain. The fluid around the unstable manifold of this central hyperbolic point (see e.g. Ottino 1989 for an introduction to chaotic advection) is expelled during the merging process and it ends up far from the final vortex. Analogously, part of the outer shells of the initial vortices gets expelled, generating the filaments that we discussed previously. The fluid coming from the two external lobes ends up in a peripheral circulation cell just around the merged core. These external lobes are reminiscent of the stable manifolds originating from the central hyperbolic point.

The picture at the level z_1', close to the top of the initial vortices, is quite different. On this level, the initial potential vorticity does not generate a final core, and all PV ends up in spiral-shaped filaments. Figure 10(*b*) confirms this picture. The particles moving to the centre of the domain, above the top of the final vortex found at lower levels, come from two complex kidney-shaped regions apparently connected with the stable manifold of the central hyperbolic point. Particles inside the initial vortices do not play a significant role, as some of them migrate toward the centre of the domain while others are expelled toward external regions. This complex behaviour is in line with the complicated structures observed in the vertical sections of the flow evolution.

4.4. *Critical merging distance*

The study of vortex merging in barotropic flows has indicated the existence of a critical distance, $d_c \approx 3.3R$ for isolated, equal patches of constant vorticity on the infinite domain. Above this distance apart, vortices do not merge and simply rotate around each other. Here, we extend this study to the case of equal ellipsoidal vortices in continuously stratified flow, and explore the dependence of the critical merging distance on the vertical aspect ratio of the initial vortices.

To this end, we consider vortices with different vertical aspect ratio and different initial separation, and measure the time they take to achieve complete merging.

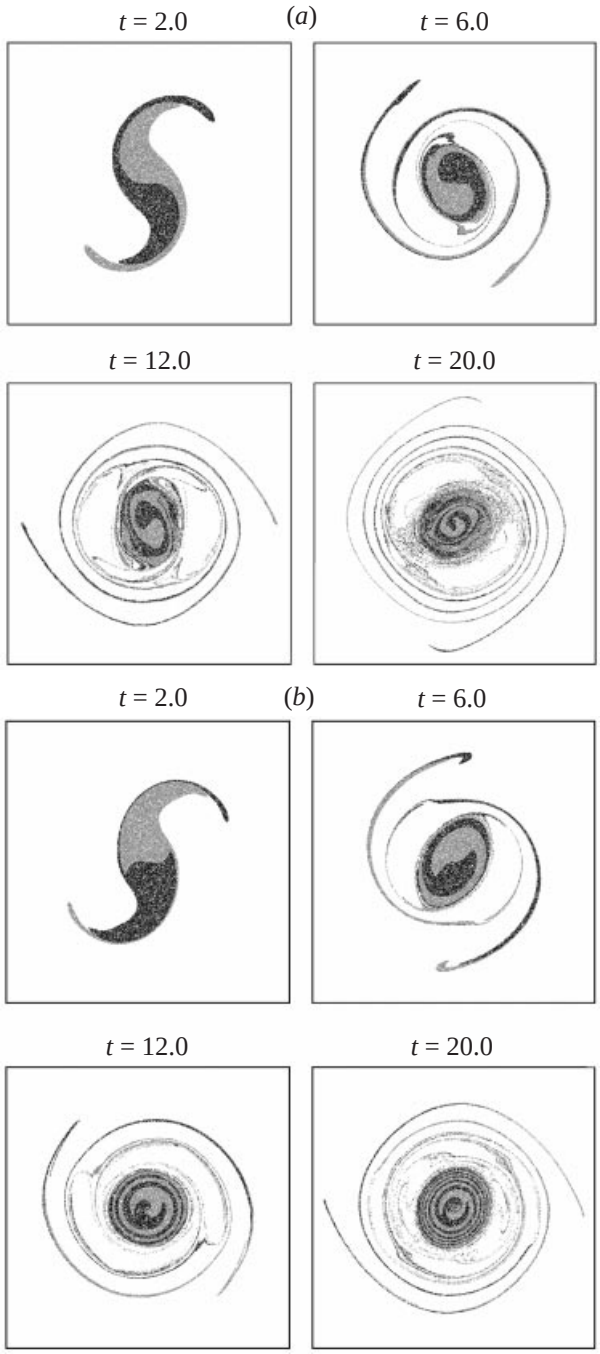

FIGURE 9(*a*, *b*). For caption see facing page.

A first problem in this context is the definition of merger itself. One option is to use a definition based on the amount of circulation trapped at the centre of the domain, or study the stability of steadily rotating equilibria (Dritschel 1985). However, Lagrangian tracers provide a simple alternative method. As shown above,

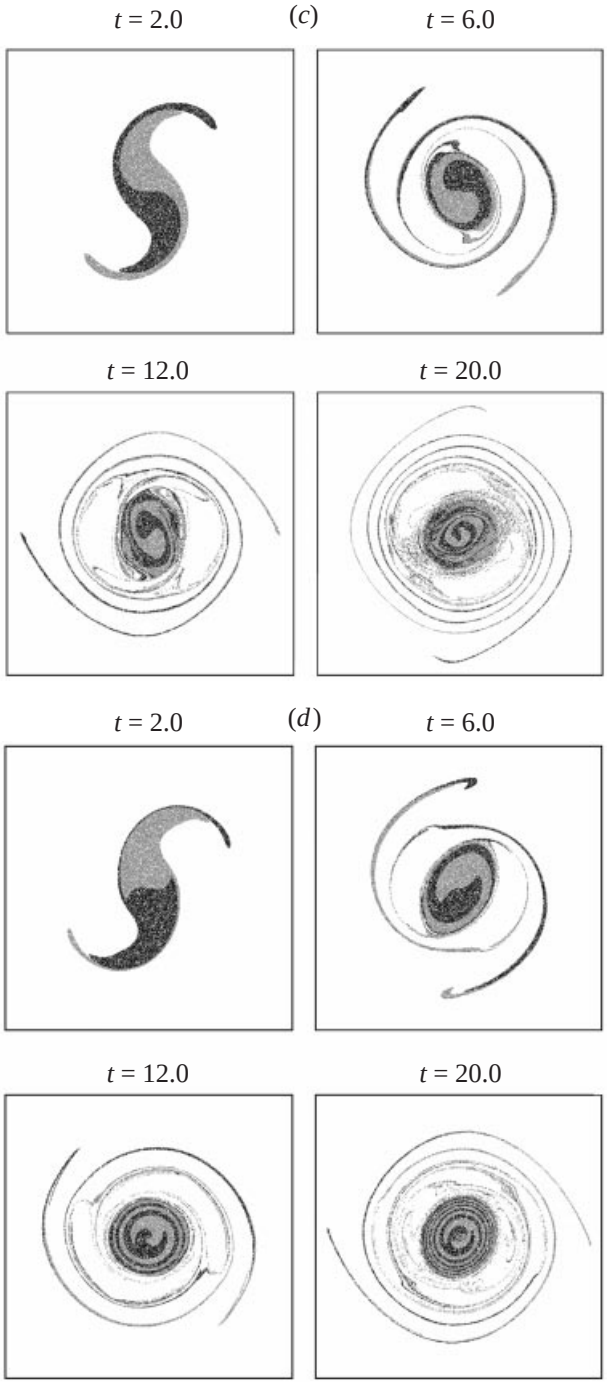

FIGURE 9. Distribution of $N = 32\,768$ passive particles initially seeded inside the two vortex cores on the central plane z'_c. The two shades of grey mark the populations seeded in the two initial cores. Times plotted are $t = 2, 6, 12, 20$. (*a*) Barotropic case, (*b*) $H/R = 1.5$, (*c*) $H/R = 0.66$, (*d*) $H/R = 0.16$.

(*a*)

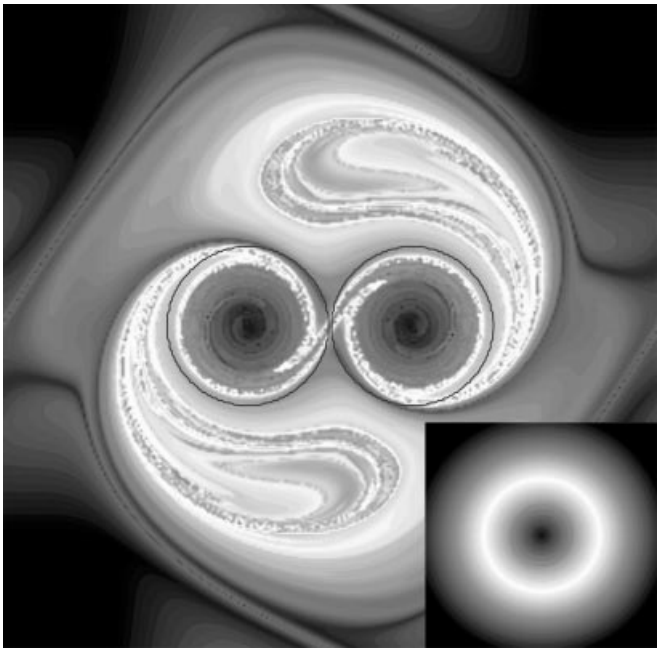

(*b*)

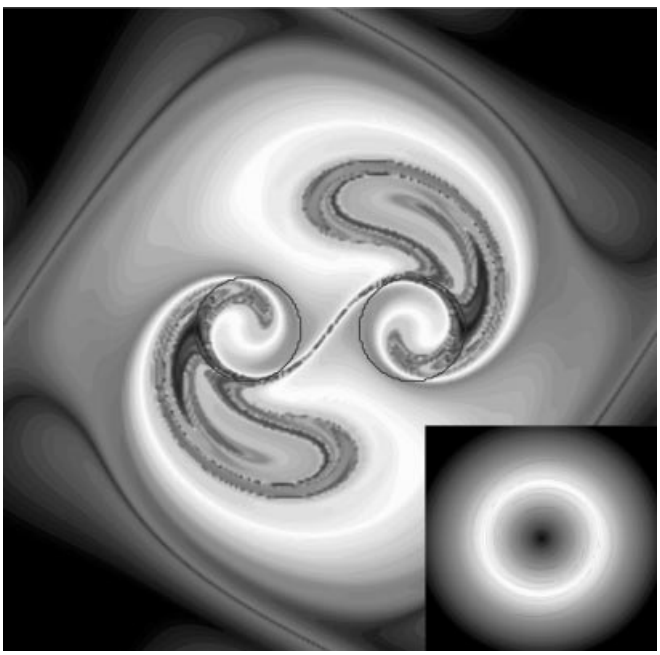

FIGURE 10. Initial tracer distribution for $H/R = 1.5$. The grey scale indicates the final distance from the centre of the domain that the particles will achieve at the end of the merging process, as depicted in the smaller panel inset. (*a*) $z_c' = D/2$, (*b*) $z_1' = D/2 + 3H/4$.

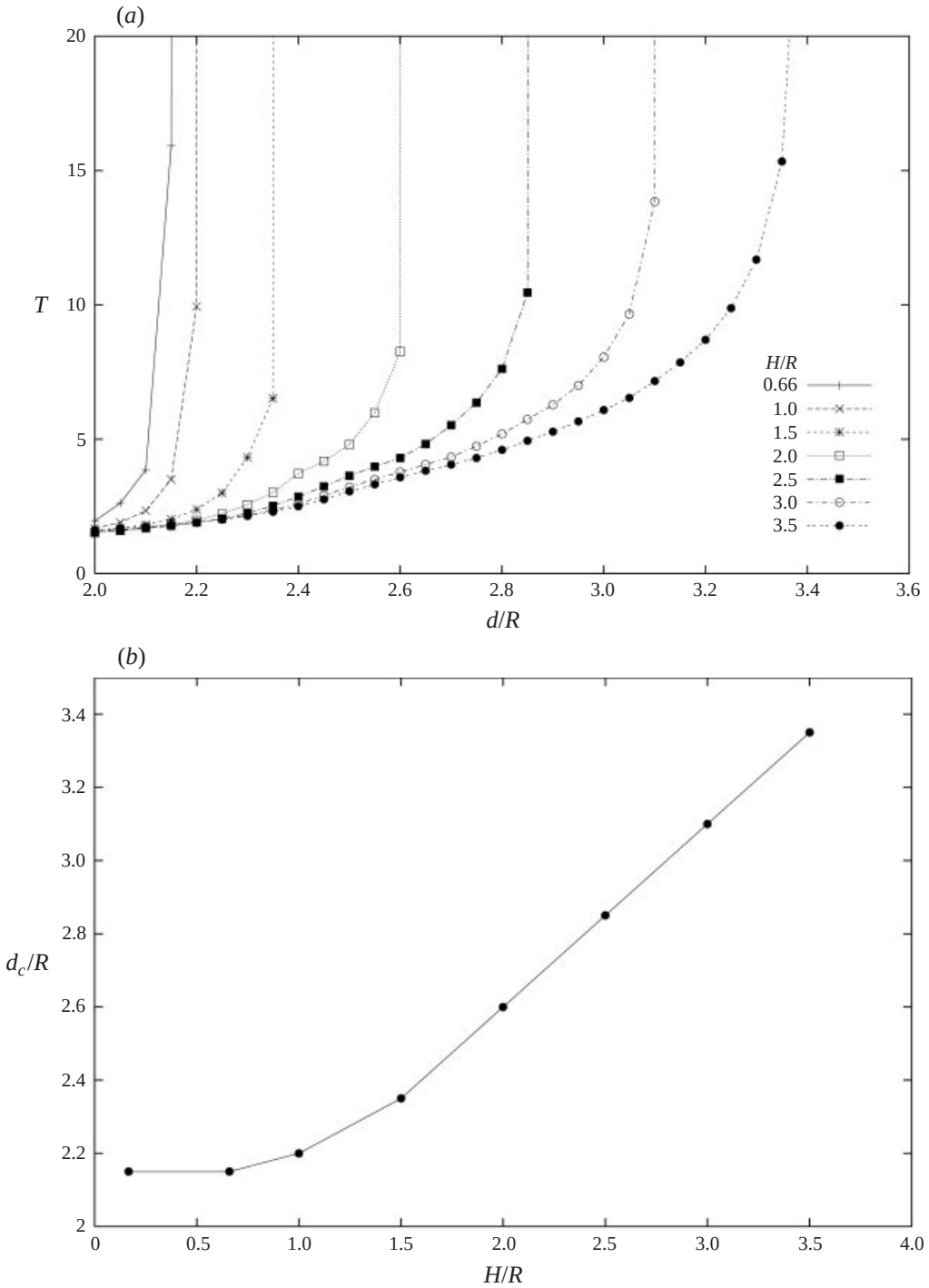

FIGURE 11. (*a*) Time to merge as a function of initial vortex distance apart, for different values of the initial vertical aspect ratio H/R, as indicated in the legend. The value of d/R for which the curve tends to infinity provides an estimate of the critical merging distance $d_c(H/R)$. (*b*) Critical merging distance $d_c(H/R)/R$ as a function of the initial vertical aspect ratio H/R.

the core of the final vortex is composed mainly of fluid originating in the cores of the two merging vortices. Thus, by marking the fluid particles in the merging cores, and tracking when most of the particles reach the central region of the domain (where the final vortex produced by merging resides), we can determine whether and when merging has taken place. Operationally, we seed a number of passive tracer particles in two small disks with radius $r_i = c_i R,\ c_i \leqslant 1$, centred in the cores of the initial vortices on the central level z'_c. During the subsequent evolution, we count the number of particles $N_c(t)$ which reach a suitably defined central region of the domain, say a circle with radius $r_f = c_f R, c_f \leqslant 2$. When $N_c(t)$ reaches a given threshold, herein chosen to be 99% of the total number of particles seeded, we declare that merging has taken place. Other values of the threshold, around the chosen one, provide similar estimates of the merging time.

The number of tracers we use in the following experiments is $N = 1024$. We choose $c_i = \frac{1}{4}$ and $c_f = \frac{3}{4}$ and explore different initial vortex separations, at different vertical aspect ratios ($H/R = 0.66, 1, 1.5, 2.5, 4$). Due to the large number of cases we have to consider, we use a smaller resolution of $128 \times 128 \times 64$ grid points. The lower resolution influences only the details of the merging, without strongly influencing the estimate of $d_c(H/R)$. A test run with resolution $256 \times 256 \times 64$ grid points, $H/R = 1.5$ and $d = 2.3R$, has provided the same estimate of the critical merging distance as the lower resolution case. In figure 11(*a*), we plot the time to merge (as defined above) as a function of the initial separation, for the different vertical aspect ratios considered.

For each value of the initial vertical aspect ratio, the time to merge increases monotonically and then tends to infinity in correspondence with the critical merging distance $d_c(H/R)$. Figure 11(*b*) shows the critical merging distance as a function of the vertical aspect ratio. These results show that baroclinicity has a strong influence on the value of $d_c(H/R)$. At low vertical aspect ratio, interactions are more local and the critical merging distance is as low as $d_c(0.66) \approx 2.1R$. As the vortices get taller, $d_c(H/R)$ increases, becoming even larger than that obtained for barotropic vortices. This behaviour, observed by Verron *et al.* (1990) for two-layer vortices, here is complicated by the fact that tall vortex columns become considerably distorted during the evolution, and the central level (where relative vorticity is maximum) can undergo merging before the higher and lower levels. At still larger values of H/R, for which vorticity is approximately constant on different levels, $d_c(H/R)$ decreases to the value appropriate for barotropic vortices (Verron *et al.* 1990). We also performed numerical simulations on the merging of top-hat vortices with the same size and amplitude as the cosine-shaped vortices considered above. For top-hat vortices, the critical merging distance is larger, as expected given their larger 'effective' radius, but the dependence of d_c on the aspect ratio mirrors that observed for cosine-shaped vortices. This suggests that the form of $d_c(H/R)$ obtained for cosine-shaped vortices properly represents the general behaviour of the critical merging distance for baroclinic vortices, independent of their detailed shape.

5. Conclusions

In this paper, we have studied merging of equal vortices lying on the same vertical level, in three-dimensional quasi-geostrophic flow. Our results indicate that there are important differences between the case with continuous stratification (as resolved by a sufficient number of vertical levels) and two-layer dynamics.

The merging of tall (or even spherical) vortices induces a decrease of the vertical aspect ratio, leading to a flatter final vortex. The vorticity filaments which are ejected

become curved in the vertical, generating a spiralling envelope around the merging vortices. The dynamics of the two merging cores is different from its barotropic counterpart, with a much more complex structure in the interior of the final vortex. This may lead to a more rapid homogenization of the core, due to small-scale mixing and diffusive effects, for baroclinic vortices than for barotropic ones.

For flat initial vortices (e.g. $H/R = 0.66$), the filaments undergo a shear instability that generates secondary vortices, which live long and trap fluid in their cores. This instability has been shown to be essentially barotropic, possibly associated with the more local nature of interactions in stratified fluids.

Consideration of the dynamics of passively advected particles has allowed better characterizing of the core dynamics, and determining the source regions of the fluid entrained in the final vortex core. Passive particle dynamics is also valuable for quantitatively determining the merging time. A study of the critical merging distance for three-dimensional vortices has indicated that flat vortices need to be much closer than tall ones in order to undergo merging.

We are grateful to JILA and Professor Juri Toomre for hospitality during part of this work, and to Bach Lien Hua for interesting discussions. The numerical computations discussed here have been performed at the Laboratory for Computational Dynamics (LCD), JILA and at the Computing Center of the Istituto di Cosmogeofisica. J. B. W. is partially supported by NSF grant OCE-9818839. J. C. M. and A. S. are partially supported by grant ONR N00014-98-1-0165.

REFERENCES

Babiano, A., Boffetta, G., Provenzale, A. & Vulpiani, A. 1994 Chaotic advection in point vortex models and two-dimensional turbulence. *Phys. Fluids* **6**, 2465–2474.

Bengtson, L. & Lighthill, J. (Eds) 1982 *Intense Atmospheric Vortices*. Springer.

Carnevale, G. F., McWilliams, J. C., Pomeau, Y., Weiss, J. B. & Young, W. R. 1991 Evolution of vortex statistics in two-dimensional turbulence. *Phys. Rev. Lett.* **66**, 2735–2737.

Charney, J. G. 1971 Geostrophic turbulence. *J. Atmos. Sci.* **28**, 1087–1095.

Dritschel, D. G. 1985 The stability and energetics of corotating uniform vortices. *J. Fluid Mech.* **157**, 95–134.

Dritschel, D. G. 1989 On the stabilization of a two-dimensional vortex strip by adverse shear. *J. Fluid Mech.* **206**, 193–221.

Dritschel, D. G. 1995 A general theory for two-dimensional vortex interactions. *J. Fluid Mech.* **293**, 269–303.

Dritschel, D. G., Haynes, P. H., Juckes, M. N. & Shepherd, T. G. 1991 The stability of a two-dimensional vorticity filament under uniform strain. *J. Fluid Mech.* **230**, 647–665.

Dritschel, D. G. & Saravanan, R. 1994 Three-dimensional quasi-geostrophic contour dynamics, with an application to stratospheric vortex dynamics. *Q. J. R. Met. Soc.* **120**, 1267–1297.

Elhmaidi, D., Provenzale, A. & Babiano, A. 1993 Elementary topology of two dimensional turbulence from a lagrangian viewpoint and single particle dispersion. *J. Fluid Mech.* **257**, 533–558.

Flierl, G. R. 1987 Isolated eddy models in geophysics. *Ann. Rev. Fluid Mech.* **19**, 493–530.

Griffiths, R. W. & Hopfinger, E. J. 1987 Coalescing of geostrophic vortices. *J. Fluid. Mech.* **178**, 73–97.

Held, I. M., Pierrehumbert, R. T., Garner, S. T. & Swanson, K. L. 1995 Surface quasi-geostrophic dynamics. *J. Fluid. Mech.* **282**, 1–20.

Hopfinger, E. J. & Heijst, G. J. F. van 1993 Vortices in rotating fluids. *Ann. Rev. Fluid Mech.* **25**, 241–289.

Hua, B. L. & Haidvogel, D. B. 1986 Numerical simulations of the vertical structure of quasi-geostrophic turbulence. *J. Atmos. Sci.* **43**, 2923–2936.

Ingersoll, A. P. 1990 Atmospheric dynamics of the outer planets. *Science* **248**, 308–315.

Kevlahan, N. K.-R. & Farge, M. 1997 Vorticity filaments in two-dimensional turbulence: creation, stability and effect. *J. Fluid Mech.* **346**, 49–76.

Kraichnan, R. H. & Montgomery, D. 1980 Two-dimensional turbulence. *Rep. Prog. Phys.* **43**, 547–619.

Leonard, B. P. 1979 A stable and accurate convective modelling procedure based on quadratic upstream interpolation. *Comp. Meth. Appl. Mech. Engng* **19**, 59–98.

McIntyre, M. E. 1989 On the antartic Ozone Hole. *J. Atmos. Terr. Phys.* **51**, 29–43.

McWilliams, J. C. 1984 The emergence of isolated, coherent vortices in turbulent flows. *J. Fluid Mech.* **146**, 21–43.

McWilliams, J. C. 1989 Statistical properties of decaying geostrophic turbulence. *J. Fluid Mech.* **198**, 199–230.

McWilliams, J. C. 1990 The vortices of geostrophic turbulence. *J. Fluid Mech.* **219**, 387–404.

McWilliams, J. C. & Weiss, J. B. 1994 Anisotropic geophysical vortices. *Chaos* **4**, 305–311.

McWilliams, J. C., Weiss, J. B. & Yavneh, I. 1994 Anisotropy and coherent vortex structures in planetary turbulence. *Science* **264**, 410–413.

McWilliams, J. C., Weiss, J. B. & Yavneh, I. 1999 The vortices of homogeneous geostrophic turbulence. *J. Fluid Mech.* **401**, 1–26.

Meacham, S. P. 1993 The merger of three dimensional, quasigeostrophic vortices in a stratified fluid. *Unpublished manuscript*.

Meacham, S. P., Pankratov, K. K., Shchepetkin, A. F. & Zhmur, V. V. 1994 The interaction of ellipsoidal vortices with background shear flows in a stratified fluid. *Dyn. Atmos. Oceans* **27**, 167–212.

Melander, M. V., Zabusky, N. J. & McWilliams, J. C. 1987 Axisymmetrization and vorticity gradient intensification of an isolated two-dimensional vortex through filamentation. *J. Fluid Mech.* **178**, 137–159.

Melander, M. V., Zabusky, N. J. & McWilliams, J. C. 1988 Symmetric vortex merger in two dimensions: causes and conditions. *J. Fluid Mech.* **195**, 303–340.

Nielsen, A. H., He, X., Rasmussen, J. J. & Bohr, T. 1996 Vortex merging and spectral cascade in two-dimensional flows. *Phys. Fluids* **8**, 2263–2265.

Ottino, J. 1989 *The Kinematics of Mixing: Stretching, Chaos, and Transport*. Cambridge University Press.

Pedlosky, J. 1987 *Geophysical Fluid Dynamics*. Springer.

Pierrehumbert, R. T. & Swanson, K. L. 1995 Baroclinic instability. *Ann. Rev. Fluid. Mech.* **27**, 419–467.

Polvani, L. M., Zabusky, N. J. & Flierl, G. R. 1989 Two-layer geostrophic vortex dynamics. Part 1. Upper-layer V-states and merger. *J. Fluid Mech.* **205**, 215–242.

Provenzale, A. 1999 Transport by coherent barotropic vortices. *Ann. Rev. Fluid Mech.* **31**, 55–93.

Shchepetkin, A. & McWilliams, J. C. 1998 Quasi-monotone advection schemes based on explicit locally adaptive dissipation. *Mon. Weath. Rev.* **126**, 1541–1580.

Sutyrin, G. G., McWilliams, J. C. & Saravanan, R. 1998 Co-rotating stationary states and vertical alignment of geostrophic vortices with thin cores. *J. Fluid Mech.* **357**, 321–349.

Valcke, S. & Verron, J. 1997 Interactions of baroclinic isolated vortices: the dominant effect of shielding. *J. Phys. Oceanogr.* **27**, 525–541.

Verron, J. & Hopfinger, E. J. 1991 The enigmatic merging conditions of two-layer baroclinic vortices. *C. R. Acad. Sci. Paris* II **313**, 737–742.

Verron, J., Hopfinger, E. J. & McWilliams, J. C. 1990 Sensitivity to initial conditions in the merging of two-layer baroclinic vortices. *Phys. Fluids* A **2**, 886–889.

Verron, J. & Valcke, S. 1994 Scale-dependent merging of baroclinic vortices. *J. Fluid Mech.* **264**, 81–106.

Waugh, D. W. 1992 The efficency of symmetric vortex merger. *Phys. Fluids* A **4**, 1745–1758.

Waugh, D. W. & Dritschel, D. G. 1991 The stability of filamentary vorticity in two-dimensional geophysical vortex-dynamics models. *J. Fluid Mech.* **231**, 575–598.

Weiss, J. B. & McWilliams, J. C. 1993 Temporal scaling behavior of decaying two-dimensional turbulence. *Phys. Fluids* A **5**, 608–621.

Yavneh, I. & McWilliams, J. C. 1995 Multigrid solution of stably stratified flows: the quasi-geostrophic equations. *J. Sci. Comput.* **11**, 47–69.

Zabusky, N. J., Hughes, M. H. & Roberts, K. V. 1979 Contour dynamics for the Euler equations in two dimensions. *J. Comput. Phys.* **30**, 96–106.

Zouari, N. & Babiano, A. 1990 Expériences numériques Lagrangiennes à partir de modèles Eulériens. *Atmos-Ocean.* **28**, 345–364.